

E13-2010-84

A. M. Balagurov, G. D. Bokuchava, I. V. Papushkin,
V. V. Sumin, A. M. Venter*

NEUTRON DIFFRACTION POTENTIALITIES
AT THE IBR-2 PULSED REACTOR
FOR NONDESTRUCTIVE TESTING
OF STRUCTURAL MATERIALS

Submitted to «Journal of Neutron Research»

*Research and Development Division, NECSA Limited, Pretoria,
South Africa

<p>Балагуров А. М. и др. Возможности метода нейтронной дифракции на импульсном реакторе ИБР-2 для неразрушающего контроля конструкционных материалов</p> <p>Исследование остаточных напряжений с использованием нейтронной дифракции имеет большие преимущества по сравнению с другими методами благодаря высокой проникающей способности нейтронов (до 2 см для стали). В Объединенном институте ядерных исследований на импульсном реакторе ИБР-2 создан специализированный дифрактометр ФСД для исследования остаточных напряжений в перспективных материалах и объемных изделиях. Данный прибор позволяет получать дифракционные спектры высокого разрешения ($\Delta d/d \approx 4 \cdot 10^{-3}$). Система радиальных коллиматоров обеспечивает выделение в образце минимального объема для исследования $2 \times 2 \times 2$ мм. Используемая нагрузочная машина, рассчитанная на максимальную нагрузку до 20 кН, позволяет проводить измерения при температурах до 800 °С. В работе дано описание ФСД и его возможностей, а также приведены примеры выполненных экспериментов.</p> <p>Работа выполнена в Лаборатории нейтронной физики им. И. М. Франка ОИЯИ.</p>	<p>E13-2010-84</p>
<p>Препринт Объединенного института ядерных исследований. Дубна, 2010</p>	

<p>Balagurov A. M. et al. Neutron Diffraction Potentialities at the IBR-2 Pulsed Reactor for Nondestructive Testing of Structural Materials</p> <p>Neutron diffraction is widely used for investigations of residual and applied stresses in bulk materials and components. The most important factor in these investigations is the high penetration depth of neutrons (up to 2 cm for steel). At the IBR-2 pulsed reactor in Dubna the Fourier stress diffractometer (FSD) has been constructed to optimize the internal stress measurements. The FSD design satisfies the requirements of high luminosity, high resolution and specific sample environment. The collimator system guarantees a minimum gauge volume of $2 \times 2 \times 2$ mm. A mechanical testing machine allows in-situ tension or compression measurements up to a load of 20 kN and sample temperatures up to 800 °C. In the paper the current status of FSD is reported and potentialities are demonstrated with several examples of investigations performed.</p> <p>The investigation has been performed at the Frank Laboratory of Neutron Physics, JINR.</p>	<p>E13-2010-84</p>
<p>Preprint of the Joint Institute for Nuclear Research. Dubna, 2010</p>	

1. INTRODUCTION

Investigations of internal stresses using high resolution time-of-flight neutron diffraction have been introduced many years ago and became widely used due to advantages in comparison with more traditional techniques: high penetration depth, high spatial resolution, separate determination of strain anisotropy and stress distribution for individual phases in multiphase materials, possibility to investigate magnetic and nonmagnetic materials, as well as to investigate irradiative materials and components [1]. The proceedings of the last European and International Conferences on Residual Stresses (ECRS-7 and ICRS-7) include many reports on neutron scattering application for nondestructive testing.

The Frank Laboratory of Neutron Physics, JINR, Dubna, is the only scientific centre in Russia where neutron diffraction is regularly used for internal stress studies and investigation of practical components. These investigations are conducted using the correlation Fourier technique [2] at the high-flux IBR-2 reactor, which is a long pulse-type source with a pulse width of about 350 μ s for thermal neutrons. Since 1995, the high resolution Fourier diffractometer HRFD [3,4] has been put into routine operation, and recently a second Fourier instrument (FSD) dedicated to stress experiments has been constructed [5,6]. In this paper, the current status of FSD is reported on and several examples are given of typical investigations.

2. FSD DESIGN AND PERFORMANCE

The FSD design satisfies the requirements of high luminosity, high resolution, specific sample environment, wide range of accessible lattice plane spacings d_{hkl} , and detectors at fixed scattering angles $+90^\circ$ and -90° . The instrument comprises of a mirror neutron guide from the reactor core, fast Fourier chopper for neutron beam intensity modulation, VME-based RTOF analyzers for data acquisition and wide-angle aperture detector systems. A distinguishing feature of the detector system is that it includes two multi-element $\text{ZnS(Ag)}^6\text{LiF}$ scintillator-based detectors at scattering angles $+90^\circ$ and -90° with combined electronic and geometric focusing [7]. Being flexible, the scintillation screen allows each element of the detector to view the time focused surface of the scattered neutrons

at the required accuracy. At the same time, the modern electronics provides the addition of signals from separate detector elements on a single time-of-flight scale. This combination leads to a sharp increase of the solid angle of the detector system and, as a result, to an increase of its luminosity, preserving a high d -spacing resolution, i.e., $\Delta d/d \approx 4 \cdot 10^{-3}$. Using a neutron gauge volume of $2 \times 2 \times 2 \text{ mm}^3$ typical measuring time per diffraction pattern is 2 to 4 hours dependant on the scattering power of the material under investigation.

The resolution function of FSD has been determined from a high-resolution neutron diffraction pattern of an α -Fe standard sample (Fig. 1) taken with three detectors (one at $2\theta \approx 141^\circ$ and two 90° detectors) at maximum Fourier chopper speed $V_{\text{max}} = 6000 \text{ rpm}$. Results show that all detectors have sufficiently high resolution and wide enough d_{hkl} range coverage: $\Delta d/d \approx 2 \cdot 10^{-3}$ for backscattering detector and $\Delta d/d \approx 4 \cdot 10^{-3}$ for 90° detectors at $d_{hkl} = 2 \text{ \AA}$ (Fig. 2). The final electronically focused spectra possess the same level of resolution as measured with the individual detector modules.

The sample environment includes the following equipment which can be used during experiments: 5-axis goniometer facilitating sample positioning for total strain tensor measurements, two load testing machines (up to 20 and 60 kN) and a mirror furnace for material studies at temperatures up to $2000 \text{ }^\circ\text{C}$.

Within the framework of bilateral scientific cooperation between the JINR and South Africa (NRF: National Research Foundation with the involvement of NECSA) project «Neutron Scattering Applications» a new mechanical load

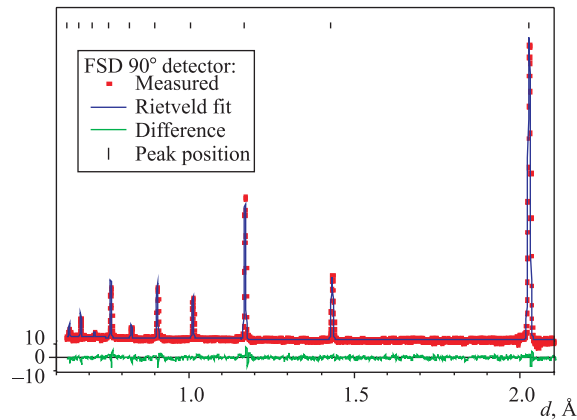


Fig. 1. Section of the neutron diffraction pattern measured from an α -Fe standard sample using the 90° detector at the maximum Fourier chopper speed $V_{\text{max}} = 6000 \text{ rpm}$. Shown are the measured data points as well as results from a Rietveld full profile analysis giving the theoretical model pattern through the data points and the difference curve between the measured and fit values

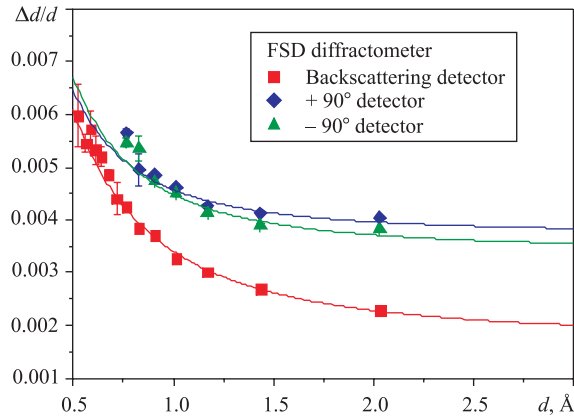


Fig. 2. Resolution function of the FSD instrument determined from the results of the α -Fe standard of Fig. 1

frame LM-20 for tensile/compressive tests with force and temperature control was purchased and incorporated on the FSD diffractometer. Furthermore, the multisection radial collimator system for the -90° detector was produced and installed.

3. RADIAL COLLIMATOR SYSTEM

The multisection radial collimator of the FSD diffractometer is designed for optimal gauge volume definition within the bulk of the sample being investigated by neutron strain scanning (Fig. 3). The radial collimator consists of 4 independent modules (two 7° and two 10° acceptance angle modules) each made of mylar foils coated with gadolinium oxide to have a total thickness of approximately $50 \mu\text{m}$. Individual modules of the radial collimator can be mechanically adjusted to optimize the geometry of the experiment (Fig. 4). All four radial collimator modules have been constructed and manufactured at PNPI (Gatchina, Russia). Performance tests show that the radial collimator provides 2 mm space resolution and

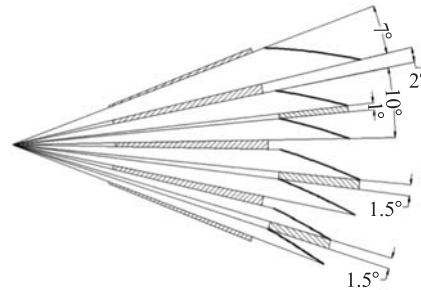


Fig. 3. Multisection radial collimator arrangement showing the flexible $\text{ZnS}(\text{Ag})^6\text{LiF}$ scintillation screens of the 90° detector. Shaded areas represent the collimator and detector walls, respectively

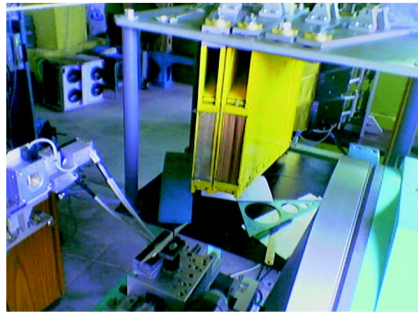


Fig. 4. Multisection radial collimator system installed on FSD rendering spatial resolution of 2 mm with the current 7 and 10° radial collimator modules

significantly improves the gauge volume definition within the bulk of the sample (Fig. 5). Residual stress depth scanning of components using the radial collimator has now become a routine procedure on FSD. In Fig. 6 the relationship between the gauge volume position and the diffraction peak intensity is shown. When the gauge volume is only partially submerged in the material, a low increase in peak intensity is observed (Region 1). When the intensity maximum is reached then the gauge volume is fully submerged (Region 2). Within this region the peak intensity exhibits exponential decrease due to neutron attenuation and scattering effects (Region 3) as function of depth below the surface. In this case the diffraction peak intensity with depth dependence is well described by the formula: $I = I_0 \exp(-\mu D)$, where μ is the linear attenuation coefficient of the material, and D is the total path length of the neutron beam within the material. Using this information the sample surface position can be determined within an accuracy of 0.1 mm (or even better with the help of the radial collimator).

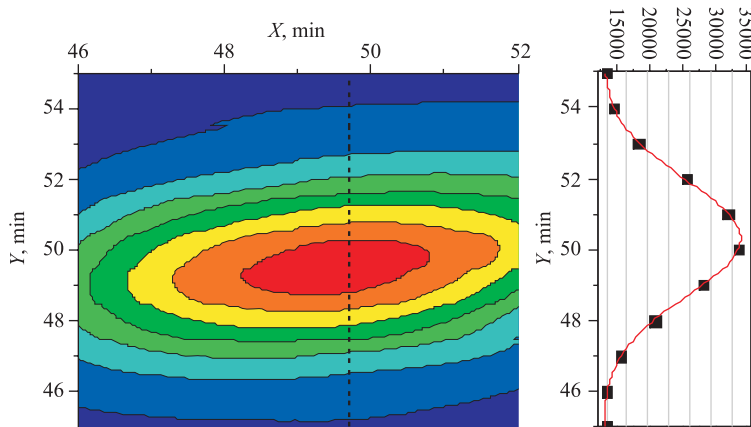


Fig. 5. Gauge volume definition: neutron intensity distribution map from the radial collimator for an incident beam width of 10 mm. Measured spatial resolution function is ≈ 2 mm

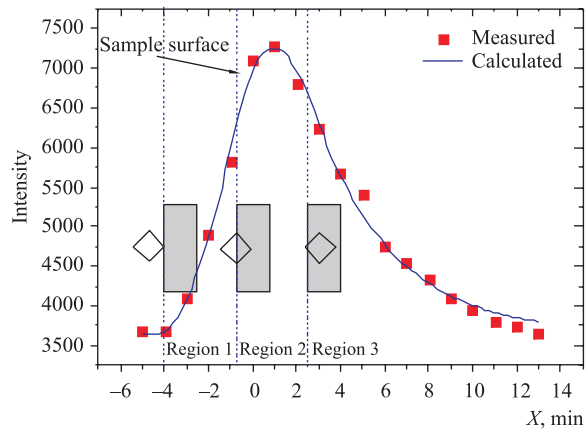


Fig. 6. Sample surface scan obtained using the radial collimator: diffraction peak intensity versus gauge volume position in the material interior

4. NEW MECHANICAL TESTING MACHINE LM-20

As a part of the sample environment modernization, a new uniaxial mechanical testing machine LM-20 was purchased from the Nuclear Physics Institute of the Czech Academy of Sciences (Rež near Prague). This instrument enables application of tensile or compressive load up to 20 kN. The main advantage of its construction is the almost play-free load transfer to the sample (Fig. 7). Additionally there is the potential to heat the sample to 800 °C (with temperature control by Eurotherm controller). LM-20 electronics can be easily integrated with FSD diffractometer control system in order to provide in-situ investigation. Samples that can be investigated need to be cylindrical ending with normal M12 screw threads for attachment to the instrument grips. Sample length between 30 and 100 mm can be accommodated (Fig. 8). Bulk sample deformation is verified by a mechanical extensometer and device control is via a PC (Windows/VME).

Main advantages of the LM-20 load frame are the load range, possibility to operate in horizontal or vertical orientation, operation at elevated temperatures, compact size, reliability, flexible software and reasonable price.

During test experiments at FLNP JINR, a steel sample was subjected to multiple tensile and compressive load cycles, load rates and amplitudes, as well as tests with heating up to 500 °C. Temperature stability during these tests was about 0.1 °C. The LM-20 machine being fully automated via the ReMeSys control software allows any combination of applied force and temperature on the sample making it applicable to a broad spectrum of potential investigations of mechanical properties of materials.



Fig. 7. Left: Picture of the uniaxial mechanical test machine LM-20: stationary part of the machine is a metallic frame consisting of two parallel platforms (1) and (2) that are connected with six cylindrical rods. Four of these rods (3) are the load-bearing elements of the construction with the remaining two (4) serving for rigid fixation of the load axis. In the centre of the bottom platform (1) is an in-line load cell for force measurement (5). (6) and (7) are upper and bottom sample grips where the sample is connected to the device (5). The upper part of the sample grip (7) is rigidly fixed to the load axis of the machine via platform (9). Load is transferred to the sample through a stepper motor, gear (10) and screw (11) mechanism. Right: View of a steel sample heated by resistive heating direct current supplied via the cables with the sample forming the heating element

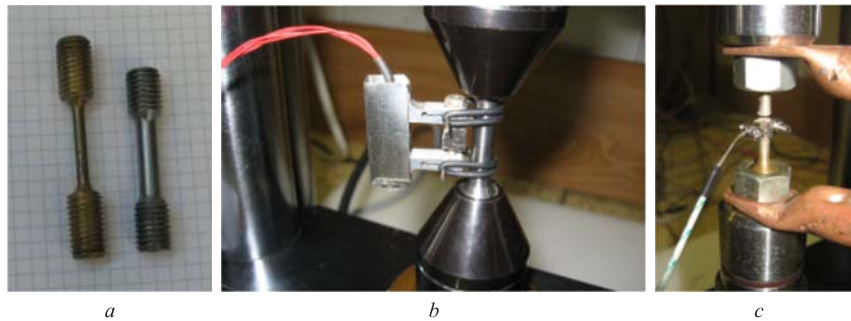


Fig. 8. Demonstration of sample setups on LM-20. From left to right: a) typical samples geometries; b) steel sample with mechanical extensometer installed; c) sample heating by direct current. The central connection is the thermocouple that is rigidly attached to the sample surface. Neutron measurements are performed on the central part of the exposed sample

5. CALIBRATION OF FSD DIFFRACTOMETER

In order to characterize FSD sensitivity to spatial strain determination inside the volume of a sample, a four-point bend experiment was performed by subjecting an aluminium alloy sample to in-situ deformation and measuring the spatial

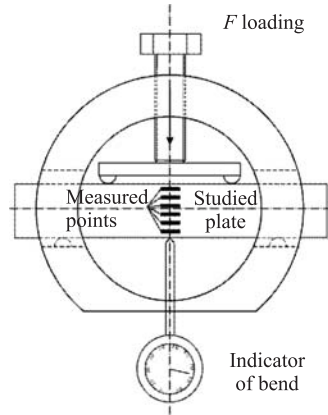


Fig. 9. Schematic of the four-point bending device. Neutron measurement points in a sample subjected to four-point bending are shown in bold

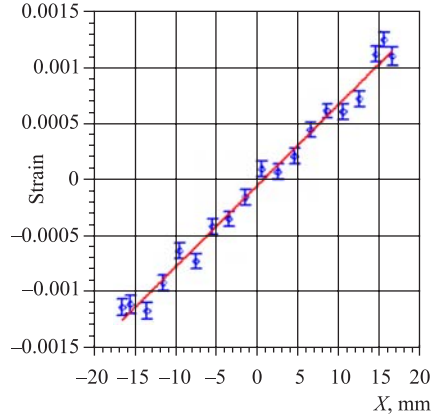


Fig. 10. Spatial distribution of the lattice strain with depth below the surface for an Al sample subjected to four-point bending. $X = 0$ corresponds to the center of the plate

strain distribution within the material with neutron diffraction (Fig. 9). According to elasticity theory, four-point bending within the elastic region induces a linear dependence through the sample thickness changing from pure tension at the bottom part to pure compression at the upper part without shear deformation.

Experimental values of lattice strains determined from diffraction peak shifts are shown in Fig. 10. The experimental uncertainties in the measured strains are 0.0001. For Al-based materials with Young's modulus in the order of 70 GPa this corresponds to a measurement accuracy of ± 10 MPa.

As further spectrometer calibration, a set of in-situ experiments to determine Young's modulus for D16 aluminum alloy (Russian grading) were performed. Samples were subjected to in-situ uniaxial tensile load using load frame installed on the sample table of FSD. Applied load was measured by a dynamometer with the total macroscopic deformation measured using a mechanical extensometer installed on the sample. Simultaneously lattice strains were measured using neutron diffraction from the relative lattice parameter change $\varepsilon = \Delta a/a$ at each value of applied stress σ ($\sigma = F/S$, where F is applied force, S is a sample cross section).

In Fig. 11 elastic lattice strain versus applied load is shown for four samples. Good agreement to the elastic theory is found with this dependence being linear for applied load up to 370 MPa. At higher load values the material undergoes plastic deformation (sample 4) which is observed as a deviation from linear dependence ($\varepsilon > 0.005$). The Young moduli were determined from curve slopes

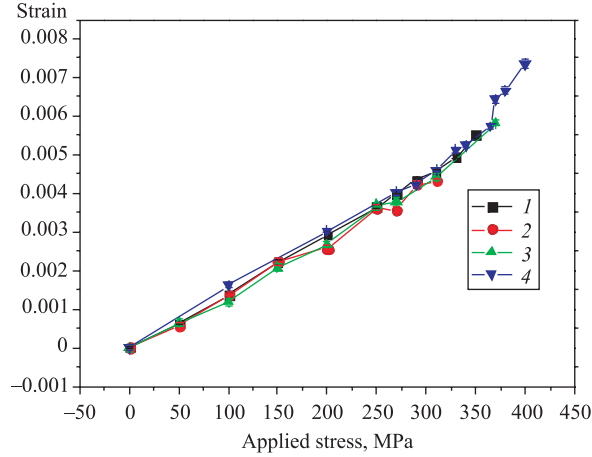


Fig. 11. Elastic lattice strain versus applied load measured in-situ on four D16 aluminum alloy samples under uniaxial tensile loading. Sample 4 undergoes plastic deformation at the highest applied load, i.e., deviation from a linear response

within the linear region. The mean value $\langle E \rangle = 68.62 \pm 0.82$ GPa compares well to the macro reference value $E = 70.3$ GPa [8]. Minor differences between measured and literature values can be ascribed to slight variation in chemical composition and thermal treatment of the samples.

6. STANDARDIZATION OF NEUTRON TECHNIQUE

In the framework of the «NET — European Network on Neutron Techniques Standardization for Structural Integrity» round robin project on sample TG1 (single weld bead-on-plate (Fig. 12)) was investigated on the FSD diffractometer [9]. Task Group 1 (TG1) has the objective to standardize residual stress measurement techniques on the benchmark, yet industrially valuable, case of a single weld bead-on-plate problem. Furthermore, TG1 aims at the equally important objective of validating the finite element method to simulate welding and predict residual stresses, by comparing predicted with measured data. All measurements were performed consistent with the recommendations stated in ISO/TTA 3:2001: Determination of Residual Stresses by Neutron Diffraction. The details of input measurements, welding, residual neutron measurements, and finite element calculations can be found in [9].

Residual strains were measured on the FSD diffractometer along the weld bead starting from $X = 0$ (center of the bead) to $X = 80$ mm (sample edge) where stresses due to the welding procedure are almost absent (Fig. 13). For

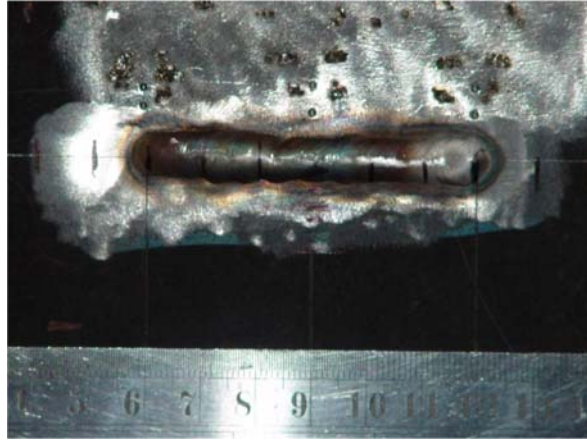


Fig. 12. Photo of single weld bead-on-plate stainless steel plate specimen (round robin sample TG1 of NET project [9]) of dimension $120 \times 180 \times 17 \text{ mm}^3$

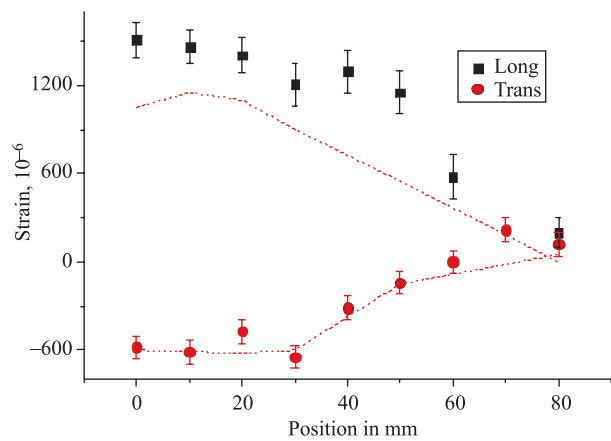


Fig. 13. Longitudinal (■) and transverse (●) strain components measured on FSD at 3 mm depth along the weld bead starting from the center of the weld. Data obtained at JRC (Petten) are represented by dashed lines

these measurements a neutron gauge volume of $3 \times 3 \times 3 \text{ mm}^3$ was defined by a boron nitride mask. The time-of-flight technique allows for the measurement of 8 reflections simultaneously. All reflections were analyzed with the Rietveld method to estimate the lattice parameter for each measurement point. Measurements away from the weld, at $X = 80 \text{ mm}$, was used as the stress-free reference of the lattice parameter. Results were in good agreement with results obtained at ISIS (UK),

NPI (Prague, Czech Republic), JRC (Petten, Netherlands) and Helmholtz-Zentrum Berlin (Germany). The observed systematical difference in longitudinal strain component could be connected with greater gauge volume used in measurements on FSD.

7. EXAMPLES OF FSD APPLICATIONS

A number of investigations are presented as examples of the typical practical applications using neutron strain scanning:

- Reactor material science: bimetallic joints [10]; austenitic build-up welds on ferritic steel; and weld seams.
- Mechanical properties of austenitic steel at various load conditions including cyclic loading [11].
- Residual stresses, phase contents and mechanical properties in new perspective materials — gradient structures and composites [12].

The results of these neutron experiments are already used for materials technology and component optimization.

Within the framework of co-operation with the Ministry of Atomic Energy of Russia, test experiments in welded VVER-1000 reactor vessel steel were car-

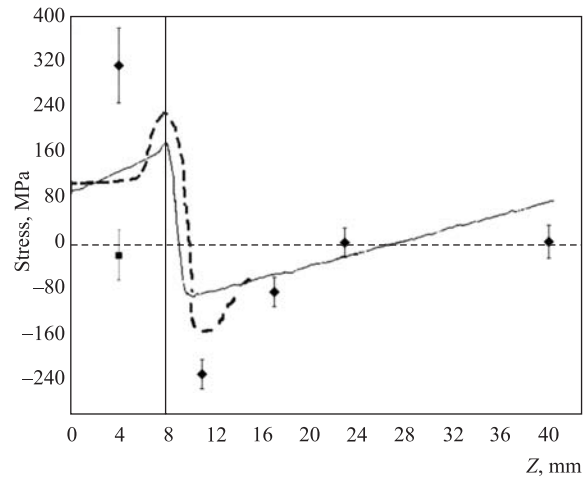


Fig. 14. Residual stresses in welded VVER-1000 reactor vessel steel template along the phase interface. The vertical line indicates the austenite–ferrite interface position at $Z = 8$ mm. Points represent residual stresses measured by neutron diffraction parallel to the phase interface (\blacklozenge — σ_y , \blacksquare — $\sigma_x \approx \sigma_z$). The dashed curve represents stress kinetic intensity value obtained using the crack propagation method while the solid curve corresponds to values estimated by cutting method

ried out. The method of welding of an austenite steel layer on a ferrite steel reactor core is frequently used to increase corrosion resistance and strengthening. Knowledge of the residual stresses in such two-layer components are important for the development of optimal strengthening built-up layers. A sample made from two steel layers: the main ferrite steel 15XГMΦAA (in Russian notation) layer 34 mm in thickness; and the welded austenite steel 12X18H10T (in Russian notation) layer with thickness of 9 mm. Residual stress results from neutron diffraction investigations and two mechanical (crack propagation and cutting) methods are shown in Fig. 14. The significant compressive σ_y stress component resulting from the build-up welding technique decreases crack corrosion probability under operating load. The partial discrepancy between the results of the different techniques can be explained by the different methodical approaches applied with the respective experimental techniques.

Austenitic stainless steels are widely used in engineering due to their high corrosion resistance and toughness. Elastic properties depend on the state of the material, chemical composition, microstructure and mechanical and thermal treatment. It is therefore essential to determine the elastic constants for the material experimentally. Neutron diffraction investigations of mechanical properties of austenitic steel under applied uniaxial load have been performed on austenitic stainless steel X6CrNiTi1810 material (wt. %) having chemical composition: C — 0.04, Si — 0.44, Mn — 1.14, P — 0.033, S — 0.004, Cr — 17.74, Ni — 19.3, Ti — 0.35. The elastic strain was measured from different crystal planes (hkl) with the scattering vector \mathbf{Q} , respectively, parallel and perpendicular to the applied load (Fig. 15). Bulk average strain was determined independently by

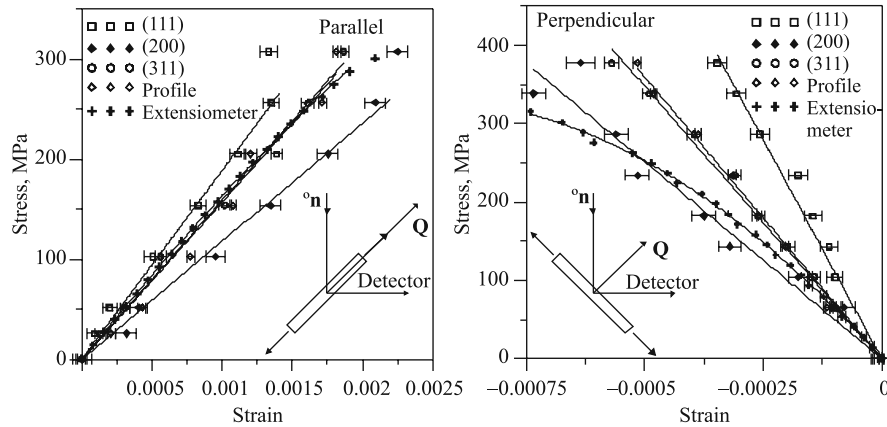


Fig. 15. Results from a neutron diffraction investigation of the mechanical properties of austenitic steel under in-situ applied uniaxial load: Lattice strain parallel (left) and perpendicular (right) to the applied load direction. The sample geometries with reference to the instrument configuration are shown in the respective inserts

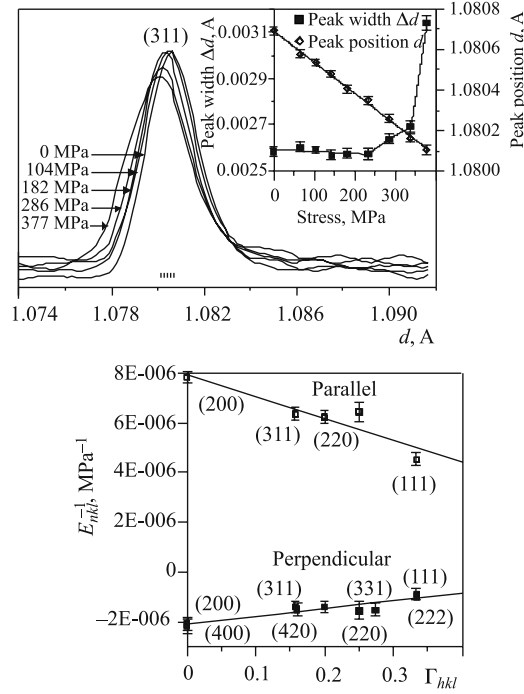


Fig. 16. Bragg reflection (311) position and width changes versus applied load (top). Dependence of the elastic modules E_{hkl}^{\parallel} and E_{hkl}^{\perp} parallel and perpendicular to the applied load versus the anisotropy factor Γ_{hkl} (bottom)

extensometers from relative changes of sample dimensions. From all diffraction patterns the diffraction peak positions and widths were determined. Diffraction patterns were also processed by the Rietveld profile refinement method that gives the strain averaged over all crystallographic directions $[hkl]$ with corresponding anisotropy factor $\Gamma_{hkl} = 0.2$. In the plastic region (applied stress level larger than ~ 250 MPa) the strain registered by the extensometer deviates from a linear dependence. Neutron diffraction data does not show strong deviation from linear dependence, but the diffraction peak widths increase significantly (Fig. 16). Such a behavior is typical for plastic deformation due to the development of microstrains (intergranular strains). In the elastic region the elastic modules E_{hkl}^{\parallel} and E_{hkl}^{\perp} as a function of the anisotropy factor $\Gamma_{hkl} = (h^2k^2 + h^2l^2 + k^2l^2)^2 / (h^2 + k^2 + l^2)^2$ were obtained from the slopes of the strain-stress linear dependences. The elastic constants S_{11} , S_{12} and S_{44} were calculated according to the Hill model [13] that ascribes taking the arithmetic average of the Reuss and Voigt model values

and gives results very close to the Kröner model values. The obtained values are in good agreement with previous studies: $S_{11} = 6.70 \cdot 10^{-6} \text{ MPa}^{-1}$, $S_{12} = -2.24 \cdot 10^{-6} \text{ MPa}^{-1}$, and $S_{44} = 12.43 \cdot 10^{-6} \text{ MPa}^{-1}$.

8. CONCLUSIONS

The investigations reported on demonstrate the FSD performance parameters and fitness for purpose to the residual stress application rendering the required 10–30 MPa accuracy. High resolution of the diffractometer ($\Delta d/d \approx 4 \cdot 10^{-3}$) allows characterization of the mechanical properties of materials at room and elevated temperatures with high precision. At the same time, spatial strain distribution studies in bulk samples is a routine procedure using the radial collimator system.

Acknowledgements. The authors wish to acknowledge the help of many members of the FLNP JINR (Dubna) and PNPI of RAS (Gatchina) staff in engineering, fabrication and installation of the FSD instrument. This work was supported within the scientific bilateral cooperation framework of the joint JINR–SA (NRF with the involvement of NECSA) project «Neutron Scattering Applications» and by IAEA under research contract No. 13737 «Application of Reverse Time-of-Flight (RTOF) Neutron Diffraction for Residual Stress Investigations».

REFERENCES

1. Measurements of Residual Stress in Materials Using Neutrons: IAEA-TECDOC-1457 // Proc. of Technical Meeting, Vienna, May 13–17, 2003. Vienna: IAEA, 2005. 92p.
2. Hiismäki P., Pöyry H., Tiitta A. // J. Appl. Cryst. 1988. V. 21. P. 349–354.
3. Aksenov V. L., Balagurov A. M., Simkin V. G. et al. // J. Neut. Res. 1997. V. 5. P. 181–200.
4. Balagurov A. M. // Neutron News. 2005. V. 16, No. 3. P. 8–12.
5. Bokuchava G. D., Aksenov V. L., Balagurov A. M. et al. // Appl. Phys. A: Mat. Sci. & Proc. 2002. V. 74 [Suppl]. P. S86–S88.
6. Balagurov A. M., Bokuchava G. D., Kuzmin E. S. et al. // Z. Kristallogr. 2006. V. 23 [Suppl]. P. 217–222.
7. Kuzmin E. S., Balagurov A. M., Bokuchava G. D. et al. // J. Neut. Res. 2002. V. 10, No. 1. P. 31–41.
8. Noyan I. C., Cohen J. B. Residual Stress Measurement by Diffraction and Interpretation. Springer-Verlag, 1987. 275 p.
9. Ohms C., Wimpory R. C., Katsareas D. E. et al. // Int. J. Press. Vessels and Piping. 2009. V. 1. P. 133–230.
10. Tamonov A. V., Sumin V. V. // J. Neut. Res. 2004. V. 12, No. 1–3. P. 69–73.

11. *Bokuchava G. D., Luzin V. V., Schreiber J. et al. // Textures and Microstructures. 1999. V. 33. P. 279–289.*
12. *Bokuchava G. D., Schreiber J., Shamsutdinov N. et al. // Physica B: Condensed Matter. 2000. V. 276–278. P. 884–885.*
13. *Hill R. // Proc. Phys. Soc. A. 1952. V. 65. P. 349–354.*

Received on July 15, 2010.

Корректор *Т. Е. Попеко*

Подписано в печать 1.10.2010.

Формат 60 × 90/16. Бумага офсетная. Печать офсетная.

Усл. печ. л. 1,18. Уч.-изд. л. 1,61. Тираж 305 экз. Заказ № 57103.

Издательский отдел Объединенного института ядерных исследований
141980, г. Дубна, Московская обл., ул. Жолио-Кюри, 6.

E-mail: publish@jinr.ru

www.jinr.ru/publish/